Methanesulfinic Acid Reaction with OH: Mechanism, Rate Constants, and Atmospheric Implications

Núria González-García, Àngels González-Lafont,* and José M. Lluch

Departament de Química, Universitat Autònoma de Barcelona, 08193 Bellaterra, Barcelona, Spain

Received: March 21, 2007; In Final Form: June 2, 2007

The mechanism for the atmospheric oxidation of methanesulfinic acid (MSIA) has been studied. This is the first theoretical study of the reaction between MSIA and the OH radical. All the possible channels in this reaction have been studied theoretically, and their corresponding rate constants have been evaluated under the variational transition-state theory (VTST) formalism. Two different products can be formed: the $CH_3S(O)_2$ radical (which had been experimentally proposed as the only one), and sulfurous acid (H_2SO_3). The $CH_3S(O)_2$ radical can be formed directly or can form via an intermediate adduct, which yields to the radical through the elimination of a water molecule. For the first time, it is theoretically demonstrated that SO_2 is formed in the addition channel of the DMS + OH reaction. The consequences of this result in the interpretation of the *T*-dependence of the SO_4^{2-}/MSA (methanesulfonic acid) quocient are analyzed. The competition between the unimolecular dissociation of the $CH_3S(O)_2$ radical and OH-addition to yield MSA is proposed as one of the possible multiple branching points (along the DMS + OH degradation scheme) influencing the *T*-dependence of the SO_4^{2-}/MSA relation.

1. Introduction

Dimethyl sulfide (DMS) is the largest natural contributor to sulfur in the troposphere.[1] It has been suggested that its atmospheric oxidation may play an important role in the formation of clouds by the production of new sulfate particles (the principal component of non-sea-salt (nss) aerosols), which act as cloud condensation nuclei (CCN) in the marine boundary layer.[2] In fact, the coupling between DMS degradation scheme and aerosols formation has been classified as an important component of the planetary climate system.[3] The main initiation step of the DMS oxidation is the reaction with OH, which proceeds by a two-channel mechanism (H-abstraction vs OH-addition).[4]

Methanesulfinic acid (MSIA) is produced in the gas-phase oxidation of DMS by OH radicals along the OH-addition branch. This idea was first proposed by Yin et al.,[5] and according to their reaction scheme, part of the DMS is oxidized to DMSO, which is then further oxidized to MSIA. Also according to their estimations, the product yield from the reaction between DMSO and OH should be 70% MSIA. In a later study by Hertel et al.,[6] based on part on the reaction scheme of Yin et al.,[5] it was found that MSIA could indeed be a very important product/intermediate in the atmospheric oxidation of DMS. They calculated that MSIA could be present in the atmosphere in concentrations comparable to MSA (methanesulfonic acid).

Sørensen et al.[7] observed for the first time MSIA formation from the reaction of DMS + OH, but with a low yield. A proposed mechanism leading to MSIA[7] is the decomposition of the adduct formed by the addition of OH to DMSO, according to the following process:

$$CH_3S(O)CH_3 + OH \rightleftharpoons CH_3S(O)(OH)CH_3 \rightarrow CH_3S(O)OH + CH_3$$

However, more recently, Arsene et al.[8] and Urbanski et al.[9] reported much higher yields of MSIA, which come from secondary oxidation of DMSO. Improvements in the experimental methods used by Sørensen et al.[7] have been recently invoked to explain those discrepancies.[4]

The reaction of MSIA with OH was proposed[7] to proceed via the formation of $CH_3S(O)_2$ radical as shown in the next reaction:

$$CH_3S(O)OH + OH \rightarrow CH_3S(O)_2 + H_2O \qquad \text{(R1a)}$$

This suggests that MSIA could be an important intermediate for the $CH_3S(O)_2$ formed within the OH-addition pathway of DMS. According to LeBras and co-workers,[10] formation of $CH_3S(O)_2$ may proceed not only by direct H-atom abstraction (R1a) but also by OH-addition to S followed by H_2O elimination (R1b-1).

$$CH_3S(O)OH + OH \rightleftharpoons CH_3S(O)(OH)_2 \rightarrow CH_3S(O)_2 + H_2O \qquad \text{(R1b-1)}$$

Flyunt et al.,[11] using a pulse radiolysis technique of aqueous solutions, proposed that MSIA behaves in many aspects like DMSO; i.e., the OH radical reacts preferentially by addition and subsequent fragmentation, giving rise, in the case of MSIA, to either methanesulfonyl (by reaction R1b-1) or methyl radicals:

$$CH_3S(O)OH + OH \rightleftharpoons CH_3S(O)(OH)_2 \rightarrow CH_3 + H_2SO_3 \qquad \text{(R1b-2)}$$

However, neither H_2SO_3 nor CH_3 radical have been actually detected in the gas phase.

Finally, the H-abstraction from the CH_3 group in MSIA could be another route of the reaction between MSIA + OH:

$$CH_3S(O)OH + OH \rightarrow CH_2S(O)(OH) + H_2O \qquad \text{(R1c)}$$

* Corresponding author. E-mail: angels@qf.uab.es.

10.1021/jp0722455 CCC: $37.00
Published on Web 07/17/2007

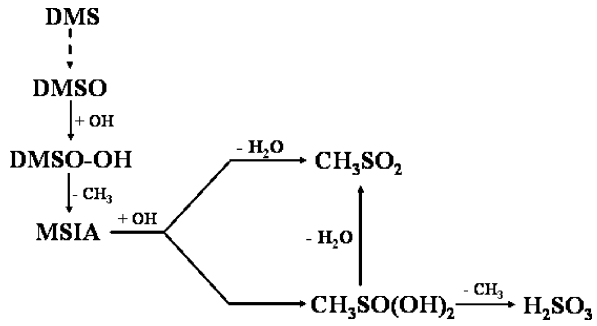

Figure 1. Schematic representation of the reactions involved in the MSIA formation in the atmosphere and the main routes of its reaction with hydroxyl radical.

However, Yin et al.[5] performed bond dissociation energy (BDE) calculations to show that the $CH_3S(O)O-H$ bond is weaker than the $H-CH_2$ S(O)OH bond, which supports the hypothesis that reaction R1c is negligible. In Figure 1 a schematic representation of the reactions already described above is shown.

The interpretation of the variation with temperature of field observables, such as the nss-SO_4^{2-}/MSA ratio, from DMS-oxidation end products has frequently been used to assess the effect of DMS on Earth's climate. The importance of this ratio is related to the availability of aerosols, fog, and clouds, and the stability of the gas-phase species that are taken up by the condensed medium. However, the final distribution of oxidized sulfur-based products under various atmospheric conditions is still controversial due to the many branching points in the DMS degradation mechanism. The initial two-channel reaction between DMS and OH is one of the important branching points in the DMS mechanism. For this reason, the nss-SO_4^{2-}/MSA ratio in both marine aerosols and ice cores had been thought to reflect the effects of the change from a predominantly H-abstraction mechanism at high temperatures to a predominantly addition mechanism at lower temperatures.[12−14] In these interpretations, sulfate formation was thought to be associated with the H-abstraction channel and MSA would be formed in the addition channel. Hynes et al.[15] and Ravishankara and coworkers[16] calculated this branching ratio from the rate constants obtained in their respective models. Ravishankara and coworkers[17] finally concluded that their calculated branching ratios between the initial H-abstraction and OH-addition could not explain the large increase in the nss-SO_4^{2-}/MSA ratio with increasing temperature. They proposed the oxidation of CH_3S (formed along the abstraction pathway) to CH_3SO_x as the key branch point to explain the field observations in DMS oxidation. Barone et al.[18] also concluded that the *T*-dependence of H-abstraction vs OH-addition is not strong enough to completely rationalize the variations in the nss-SO_4^{2-}/MSA ratios observed in the ice cores and with latitude. They suggested that the steep temperature-dependent branching ratio between SO_2 and MSA could be a result of the competition between the unimolecular dissociation of the $CH_3S(O)_2$ radical, leading to SO_2 and then H_2SO_4, and the reaction of this radical with O_3 to further oxidize the sulfur atom without breaking the S−C bond, leading to MSA. The *T*-dependence of the atmospheric nss-SO_4^{2-}/MSA branching was shown to reflect the activation energy for the $CH_3S(O)_2$ dissociation (see Figure 4 in ref 18). As the reaction between MSIA + OH leads to $CH_3S(O)_2$ (see reactions R1a and R1b-1), so connecting the OH-initiated addition branch with the OH-initiated abstraction branch of the DMS degradation mechanism, it might be a crucial process to understand the end-products distribution of the DMS oxidation, and in particular, the nss-SO_4^{2-}/MSA ratio found in the atmosphere.

In our laboratory, we have performed several studies following the different reactions along the OH-addition and H-abstraction pathways of DMS atmospheric oxidation.[19−21] We first characterized the initiation routes of the DMS atmospheric oxidation by reaction with OH.[19,20] Our calculations showed that, in the absence of oxygen, the main reaction is the H-abstraction channel, in good agreement with experimental observations. Although the OH-adduct is formed, it does decompose back to reactants because the fragmentation reaction (to form $CH_3SOH + CH_3$) is very slow. In the presence of oxygen the situation is completely different. The oxygen scavenges the $CH_3S(OH)CH_3$ adduct very fast to mainly form DMSO.[16,22]

The reaction between DMSO and OH has been found to be very fast, so this removal process is likely to be the dominant atmospheric sink of DMSO. As indicated above, there is now a general agreement that MSIA is one of the products from the OH-initiated oxidation of DMSO.[8,9] Very recently, we performed a theoretical study on the mechanism of the DMSO + OH reaction and we found the branching ratio for the MSIA production was around 98% at 298 K,[21] in good agreement with the experimental yield of 0.9 ± 0.2 at the same temperature.[1]

In this paper we will present the results obtained for the MSIA + OH reaction, mainly focusing in the mechanism and kinetics of $CH_3S(O)_2$ formation; we will also discuss the possible role of this radical in the nss-SO_4^{2-}/MSA ratio. This work supposes the final step in the studies we have already performed regarding the OH-addition channel in the DMS + OH atmospheric oxidation.

2. Methods of Calculation

2.1. Electronic Structure Calculations. Geometry optimization, energies, and first and second energy derivatives for the different stationary points involved in the reactions proposed were calculated by using the modified Perdew−Wang one-parameter model for kinetics (mPW1K) functional[23] with the MG3S basis set.[24,25] This functional has been optimized to a database of barrier heights and reaction energetics[26] and shows a good compromise between cost and accuracy in describing heavy atom transfer reactions,[27] nonbonded interactions,[26,28] and $\pi-\pi$ interactions.[29,30] The MG3S basis set[24] was chosen as the best one for our system. This MG3S basis works specially well for describing sulfur-containing molecules because it includes tight d functions that seem to be a prerequisite for consistent accuracy on second-row atoms. The MG3S basis satisfies this criterion (the exponent of the tighest *d* function for S is 2.6).[25] The nature of the stationary points has been determined by means of the analysis of the number of imaginary frequencies: NIMAG = 1 for a saddle point (SP) or NIMAG = 0 for minima. Energies at all the stationary points were then recalculated at the higher level of theory: CCSD(T)/IB, from Truhlar and coworkers,[31,32] where the CCSD(T) stands for coupled cluster approach with single and double excitations and quasiperturbative connected triples, and IB stands for extrapolation to the infinite basis set. This extrapolation scheme is based only on single-point energy calculations with cc-pVDZ and cc-pVTZ basis sets. The CCSD(T) calculations are frozen core. The combination of the low-level method, mPW1K/MG3S, and the high-level method, CCSD(T)/IB, has been tested before for other reactions involved in the DMS atmospheric oxidation.[19,20]

To ensure the connectivity between the stationary points found and for their use in the dynamical calculations, the minimum energy path (MEP)[33] in an isoinertial mass-weighted Cartesian coordinate system was calculated starting from each

saddle-point geometry found, by following the Page−McIver algorithm[34] at the mPW1K/MG3S level of theory. A step size, δs, of 0.01 bohr (where s denotes the distance along the MEP in an isoinertial mass-scaled coordinate system with a scaling mass equal to 1 amu) was used in all cases. The second derivative matrix was calculated at every two points of each MEP. For the two association regions (RCabs and RCad formation) we built a distinguished reaction coordinate path (DCP) at the mPW1K/MG3S level, because those are barrierless processes, i.e., without saddle point.

The interpolated single-point energy correction (ISPE)[35] procedure was used for the variational transition-state theory calculations. Thus, in addition to the stationary points, we calculated the single-point CCSD(T) energies at several non-stationary points along the MEPs or DCPs.

The generalized normal-mode analysis along the MEPs and the DCPs was performed in mass-scaled Cartesian coordinates. The reoriented dividing surface (RODS)[36] algorithm was used to improve the generalized frequencies along the MEPs whereas along the DCPs, the algorithm becomes completely necessary to obtain reliable generalized eigenvectors and frequencies.

Geometry optimization and the Hessian matrix for stationary points, as well as CCSD(T) single-point energy calculations, were carried out with the Gaussian03 package of programs.[37] The GaussRate9.1 code,[38] which is an interface linking PolyRate9.3[39] and Gaussian03,[37] was used for calculating the information along the MEPs and DCPs at the mPW1K/MG3S level.

2.2. Dynamical Calculations. All the rate constants were calculated by means of canonical variational transition-state (CVT) theory.[40−44] The semiclassical transmission coefficient, $\kappa(T)$, which corrects the CVT rate constant to account for the quantum effects on the nuclear motion along the reaction path, was not included because those effects were not possible (none of the reaction channels presents a positive adiabatic ground-state potential energy barrier).

The CVT rate constant is defined as

$$k^{\mathrm{CVT}}(T) = \frac{k_{\mathrm{B}}T}{h}\sigma\frac{Q^{\mathrm{GT}}(T,s^*)}{Q^{\mathrm{R}}(T)}\exp(-V(s^*)/k_{\mathrm{B}}T) \qquad (1)$$

where s^* is the value of s at the free energy maximum along the reaction path (MEP or DCP) at temperature T, σ is the symmetry number, k_{B} is the Boltzmann's constant, h is Planck's constant, $V(s^*)$ is the classical potential energy at s^* with zero of energy at the overall classical energy of reactants (that is, without the ZPE corrections which will be included in the partition functions), $Q^{\mathrm{R}}(T)$ is the reactant partition function per unit volume (again with zero of energy at reactants), and $Q^{\mathrm{GT}}(T,s^*)$ is the generalized transition-state partition function with zero of energy at $V(s^*)$ and excluding the reaction coordinate. It should be noted that rotational symmetry numbers were removed for all partition functions, as they are included in σ. The description of this symmetry number can be found elsewhere.[20,21,45] In all cases the vibrational partition functions have been evaluated within the harmonic approximation. All rate constants where computed with the PolyRate9.3 code.[39]

3. Results and Discussion

In this section we will first present an electronic structure and dynamical description of the MSIA + OH reation mechanism. Next, the calculated rate constants for each individual channel as well as the global rate constants will be presented and analyzed. All the energies given in the text are adiabatic potential energies vs MSIA + OH, and correspond to the electronic-structure level CCSD(T)/IB//mPW1K/MG3S, unless otherwise is stated. All the energetic data for the different regions of both channels R1a and R1b can be found in the Supporting Information.

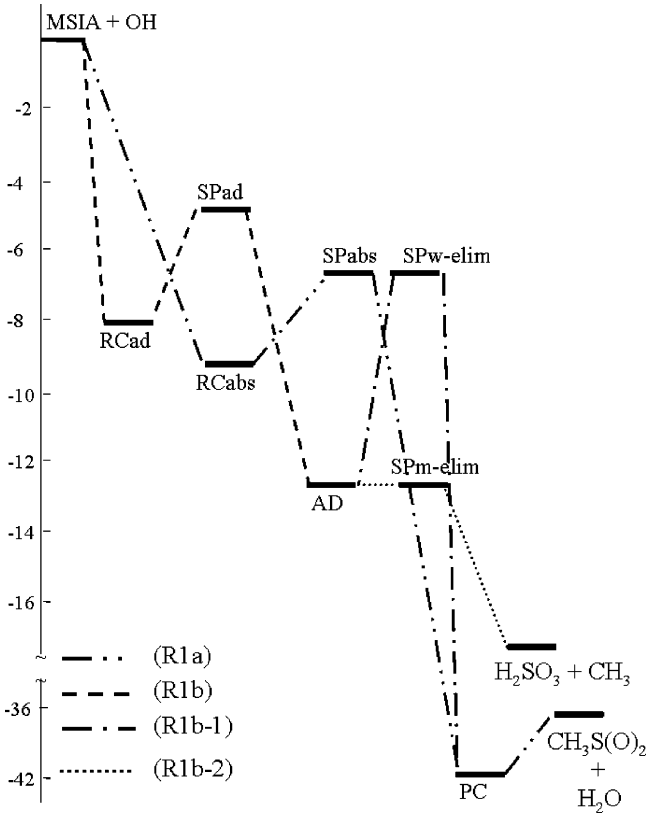

Figure 2. Adiabatic potential energy diagram (in kcal/mol) for the different stationary points of the MSIA + OH reaction. Energies have been calculated at the CCSD(T)/IB//mPW1K/MG3S level.

The different stationary points found correspond to the mechanism described in the Introduction: a H-abstraction channel (R1a), an addition−H_2O-elimination channel (R1b-1), and an addition−CH_3-elimination channel (R1b-2). The mechanism of the H-abstraction reaction (R1a) was found to proceed via a complex in the entrance channel (RCabs), followed by the saddle-point structure of this H-abstraction process (SPabs). The SPabs saddle point is connected with a complex in the exit channel (PC), which finally dissociates to form the final abstraction products: H_2O and $CH_3S(O)_2$ radical. On the other hand, in both (R1b-1) and (R1b-2), an addition-type complex (which will be called AD) is formed. The formation of this AD takes place via a previous reactant complex (RCad), quite similar to the RCabs found in the R1a channel, which through a saddle point (SPad) forms AD. Then, this AD can evolve either by water elimination, to form the abstraction products described in channel R1a (i.e., PC and after that H_2O and $CH_3S(O)_2$ radical) or by the elimination of the methyl group to form H_2SO_3 + CH_3 radical. Both the water and the methyl-elimination processes were found to proceed through a saddle point, SPw-elim and SPm-elim, respectively (where w-elim and m-elim stand for water elimination and methyl elimination, respectively). A global description of the three degradation routes for the MSIA plus OH reaction is depicted in Figure 2.

Taking into account the mechanism for the MSIA + OH reaction, and neglecting reaction R1c (the reasons have been explained before), the whole rate constant for reaction R1 will be the sum of the fluxes for each possible channel:

$$k_{\mathrm{MSIA+OH}}(T) = k_{\mathrm{R1a}}(T) + k_{\mathrm{R1b}}(T) \quad (2)$$

where $k_{\mathrm{R1a}}(T)$ and $k_{\mathrm{R1b}}(T)$ are the rate constants for the H-abstraction and the addition−elimination mechanisms, respectively.

On the basis of the experimental work published by Kukui et al.,[1] we just present here the rate constants evaluated at the low-pressure limit. In that work, the product yield of the reaction was independent of pressure in the range 200−400 Torr, and no indication of stabilized complex formation was found. Moreover, taking into account that the saddle points in all channels appear at energies quite below reactants, there are no energetic barriers that could help to stabilize the intermediates. Anyway, some results and discussion corresponding to the high-pressure limit are given as Supporting Information.

In this way, we applied the canonical unified statistics (CUS) theory[46] to obtain the rate constant for the H-abstraction channel (R1a). This theory is a canonical generalization of the microcanonical unified statistical (US) theory[47] based on the probability branching analysis of Hirschfelder−Wigner.[48] The corresponding rate constant, $k_{\mathrm{R1a}}(T)$, will be given by

$$\frac{1}{k_{\mathrm{R1a}}(T)} = \frac{1}{k_{\mathrm{assn-abs}}(T)} - \frac{1}{k_{\mathrm{RCabs}}(T)} + \frac{1}{k_{\mathrm{SPabs}}(T)} - \frac{1}{k_{\mathrm{PC}}(T)} + \frac{1}{k_{\mathrm{dissn}}(T)} \quad (3)$$

where $k_{\mathrm{RCabs}}(T)$ and $k_{\mathrm{PC}}(T)$ are the one-way flux rate constants evaluated at the complexes formed along the reaction path (RCabs and PC, respectively). In fact, none of these terms will be included because they are big enough that their inverse terms in the corresponding CUS equation become negligible. In eq 3, $k_{\mathrm{assn-abs}}(T)$, $k_{\mathrm{SPabs}}(T)$, and $k_{\mathrm{dissn}}(T)$ are the rate constants for the association (reactants → RCabs), abstraction (RCabs → PC), and dissociation (PC → products) regions, respectively, for this channel. Moreover, the dissociation region will not be included in practice in the final $k_{\mathrm{R1a}}(T)$ and $k_{\mathrm{R1b}}(T)$ evaluation due to the high exothermicity of the channel: $k_{\mathrm{PC}}(T)$ and $k_{\mathrm{dissn}}(T)$ take very high values and their contribution to the global rate constants of channels R1a and R1b becomes irrelevant.

On the other hand, to obtain the rate constant corresponding to the R1b channel (including the two different eliminations) we applied both the CUS[46] and the competitive canonical unified statistical (CCUS)[49] theories, because several bottlenecks, both consecutive and competitive, appeared. In this way, the rate constant for channel R1b is given by

$$\frac{1}{k_{\mathrm{R1b}}(T)} = \frac{1}{k_{\mathrm{assn-ad}}(T)} - \frac{1}{k_{\mathrm{RCad}}(T)} + \frac{1}{k_{\mathrm{SPad}}(T)} - \frac{1}{k_{\mathrm{AD}}(T)} + \frac{1}{k'_{\mathrm{w-elim}}(T) + k_{\mathrm{SPm-elim}}(T)} \quad (4)$$

where $k_{\mathrm{RCad}}(T)$ and $k_{\mathrm{AD}}(T)$ are the one-way flux rate constants evaluated at the complexes formed along the reaction path (RCad and AD, respectively). It should be noted that, for the same reasons explained above, $k_{\mathrm{RCad}}(T)$ and $k_{\mathrm{AD}}(T)$ have not been included. $k_{\mathrm{assn-ad}}(T)$, $k_{\mathrm{SPad}}(T)$, and $k_{\mathrm{SPm-elim}}(T)$ are the rate constants for the association (reactants → RCad), addition (RCad → AD), and methyl-elimination (AD → $H_2SO_3 + CH_3$) regions, respectively. $k'_{\mathrm{w-elim}}(T)$ includes the contribution of the two regions found in the R1b-1 channel, after the adduct formation, i.e. the water-elimination and the dissociation regions. However, as previously mentioned, the dissociation region will not be included in practice in the calculations.

$$\frac{1}{k'_{\mathrm{w-elim}}(T)} = \frac{1}{k_{\mathrm{SPw-elim}}(T)} - \frac{1}{k_{\mathrm{PC}}(T)} + \frac{1}{k_{\mathrm{dissn}}(T)} \quad (5)$$

As mentioned before, adduct AD can decompose via two different competitive processes, leading to different products. Their corresponding rate constants are obtained from eqs 6 and 7.

$$k_{\mathrm{R1b-1}}(T) = \frac{k'_{\mathrm{w-elim}}(T)}{k'_{\mathrm{w-elim}}(T) + k_{\mathrm{SPm-elim}}(T)} \cdot k_{\mathrm{R1b}}(T) \quad (6)$$

$$k_{\mathrm{R1b-2}}(T) = \frac{k_{\mathrm{SPm-elim}}(T)}{k'_{\mathrm{w-elim}}(T) + k_{\mathrm{SPm-elim}}(T)} \cdot k_{\mathrm{R1b}}(T) \quad (7)$$

All these rate constants are calculated at the corresponding bottlenecks in each region of the PES. Note that, despite the separation in different regions that we have done for each mechanism, according to the CUS theory[50] all the rate constants are calculated with respect to the same thermally equilibrated reactants, MSIA and OH, as corresponds to a low-pressure scenario.

3.1. H-Abstraction Channel (R1a). In Figure 3, the geometrical representations of the stationary points along the H-abstraction channel (R1a) are presented. First, a reactant complex (named RCabs) is formed, stabilized by 9.25 kcal/mol. This stabilization is mainly due to the two H-bonds formed between MSIA and OH, O1−H2 and H1−O3 (see Figure 3 for numbering). This last distance becomes the reaction coordinate in the next region of the PES (that corresponds to the abstraction process). The formation of this complex takes place without a potential energy barrier, and in this sense, the CVT formalism becomes necessary to calculate the rate constant for the association region. The next stationary point along the PES is the saddle point (named SPabs) corresponding to the abstraction of the H1 atom in MSIA by the OH group. The SPabs is 6.82 kcal/mol under reactants. The distance of the O2−H1 breaking bond is 1.11 Å whereas for the forming bond O3−H1 is 1.28 Å, 0.14 Å longer and 0.65 Å shorter, respectively, than those in the RCabs structure. The product complex found in the exit channel is stabilized at 42.20 kcal/mol and presents a long H-bond between O2−H1 atoms (the broken bond).

In summary, three different regions appear in the PES of the H-abstraction channel (R1a): the association region (MSIA + OH → RCabs), which does not present a maximum along the classical potential energy profile; the H-abstraction (RCabs → PC), where the dynamical bottleneck of the reaction will be situated around the SPabs structure; and the dissociation region, which represents the H-bond breaking from the PC complex, to finally form the products. As has been previously said, due to the high exothermicity of the reaction, the dissociation region will not be included in the final evaluation of the rate constant.

The rate constants for the association and abstraction regions have been calculated in the range 298−600 K, and the results can be seen in Table 1. For the RCabs formation, only the CVT rate constants can be calculated. For the abstraction region the existence of a saddle point has allowed us to calculate the rate constants using both the conventional transition-state theory (TST) and the CVT theory. This way the corresponding variational effects have been evaluated. However, they turn out to be not very important: at $T = 298$ K, they slow the rate constant by a factor of 0.80. If we compare the rate constants for the two regions, the association is always faster than the H-abstraction in all the range of temperatures analyzed. However, this ratio decreases as the temperature increases: at

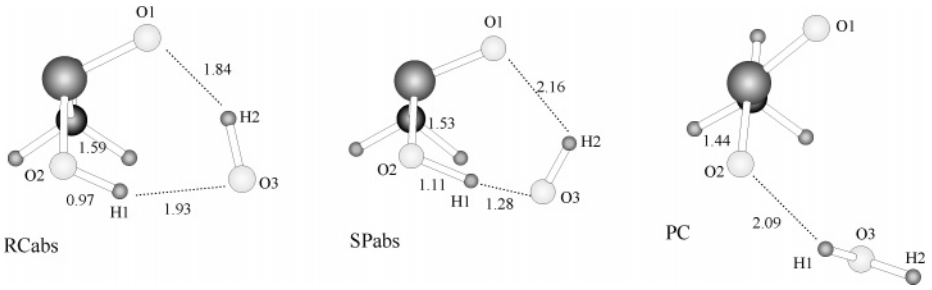

Figure 3. Geometrical representations of the complexes (RCabs and PC) and saddle point (SPabs) along the H-abstraction (R1a) channel in the MSIA + OH reaction. Distances are given in Å and angles in degrees.

TABLE 1: Rate Constants (cm^3 $molecule^{-1}$ s^{-1}) for the H-Abstraction Channel (R1a) Computed at the CCSD(T)/IB//mPW1K/MG3S Level of Theory[a]

T (K)	$k_{assn-abs}$ (T)	k_{SPabs}^{TST} (T)	k_{SPabs}^{CVT} (T)	k_{R1a} (T)
298	2.94 (−09)	7.55 (−10)	6.06 (−10)	5.02 (−10)
325	1.40 (−09)	3.78 (−10)	3.13 (−10)	2.56 (−10)
350	7.81 (−10)	2.19 (−10)	1.87 (−10)	1.51 (−10)
400	3.11 (−10)	9.25 (−11)	8.20 (−11)	6.49 (−11)
450	1.56 (−10)	4.83 (−11)	4.41 (−11)	3.44 (−11)
500	8.96 (−11)	2.92 (−11)	2.73 (−11)	2.09 (−11)
600	4.03 (−11)	1.44 (−11)	1.39 (−11)	1.03 (−11)

[a] Power of ten in parentheses.

$T = 298$ K the association rate constant is 4.9 times faster than the abstraction one, whereas at $T = 600$ K this ratio is only 2.9. For this reason, the two dynamical bottlenecks in the path must be taken into account in the calculation of the global rate constant for channel R1a. In this way, the rate constant for the direct H-abstraction, $k_{R1a}(T)$, is calculated by means of eq 3, and the results are also shown in Table 1 (last column). Following the same tendencies as the individual rate constants for each region, the $k_{R1a}(T)$ rate constant decreases as T increases.

3.2. Addition−Elimination Channel (R1b). The formation of an adduct between MSIA and OH radical, where the O3 atom in the hydroxyl radical is bonded to the S atom in MSIA, was previously proposed by Le Bras.[10] However, this adduct was neither experimentally detected nor theoretically characterized. We studied the formation of this adduct, and we found it proceeds via an initial complex, named RCad (see Figure 4), whose structure is quite similar to the RCabs geometry previously described: the RCad complex represents also a two H-bonded structure, but the H-bonds are weaker than the ones in RCabs. This difference produces a lower stabilization energy of RCad in comparison with that for RCabs: 8.14 vs 9.25 kcal/mol, respectively. The RCad complex forms the AD adduct via a saddle point (named SPad), situated 4.75 kcal/mol lower than the reactants. The geometry of AD can be seen in Figure 4. The S−O3 bond distance in the MSIA−OH adduct is 1.98 Å, much shorter than the corresponding bond (2.26 Å) in DMS−OH,[19] and quite similar to the one in the DMSO−OH adduct (1.92 Å).[20] These distances are in agreement with their relative classical potential energies of stabilization: 12.84, 8.85, and 10.85 kcal/mol, respectively (at the mPW1K/MG3S level of theory).[19,20]

The rate constants for both the association and addition regions can be seen in Table 2 (see columns 2 and 3). As the association region in channel R1a, the RCad complex is formed without any classical potential energy barrier, which means the CVT formalism should be applied to calculate the corresponding rate constant. For the addition region we have calculated both the TST and the CVT rate constants. Because the variational effects turn out to be quite small, just the CVT rate constants are shown in Table 2.

At the AD structure, this channel bifurcates following two different elimination processes. For this reason, both processes will be analyzed individually.

3.2.1. Water Elimination: Channel (R1b-1). We have confirmed the existence of a second pathway to form the $CH_3S(O)_2$ radical, via the elimination of a water molecule (i.e., an internal H-abstraction followed by the water molecule elimination) from the AD structure. The saddle point connecting this AD adduct with the corresponding PC complex (common point with the R1a channel), named SPw-elim, is depicted in Figure 4. This SPw-elim structure is 6.78 kcal/mol below reactants, but 5.62 kcal/mol above the AD complex. The saddle-point structure is characterized by the two bond distances S−O3 and S−O2, which are 0.26 Å longer and 0.45 Å shorter than in AD, respectively. The internal O3−H1 distance (the forming bond) is 1.37 Å, 0.62 Å shorter than in the AD stationary point.

The $k'_{w-elim}(T)$ rate constant (obtained by means of eq 5), together with the global rate constant for the addition−H_2O-elimination process (R1b-1) (obtained by means of eq 6) as a function of temperature are listed in Table 2. Comparing these values with the previous ones obtained for the direct H-abstraction (R1a channel) indicates this mechanism is irrelevant. Just as an example, at $T = 298$ K, the rate constant for the direct H-abstraction is 5.02×10^{-10} whereas for the R1b-1 channel it is 1.17×10^{-14} cm^3 $molecule^{-1}$ s^{-1}. In consequence, all the $CH_3S(O)_2$ radical formed in the reaction comes from the direct H-abstraction channel.

The way in which the $CH_3S(O)_2$ radical is formed will influence its excitation energy, which will be used in the decomposition of this radical to finally form SO_2. Then, to evaluate the internal energy of the $CH_3S(O)_2$ radicals we would have to take into account they are only formed by direct H-abstraction, i.e., channel R1a.

3.2.2. Methyl Elimination: Channel (R1b-2). A second possible route for the AD adduct fragmentation is the S−C bond breaking, which takes place through the SPm-elim saddle point, which connects with the products of the R1b-2 process: H_2SO_3 + CH_3. The SPm-elim structure is depicted in Figure 4, and its main characteristic is the long S−C bond, 0.48 Å longer than in the AD structure. This elongation results in the two S−OH bonds being shorter. The SPm-elim is 12.41 kcal/mol lower than reactants, and 0.01 kcal/mol lower than AD. This would mean that all the AD adduct formed will rapidly decompose to form the methyl-elimination products. The rate constant for the methyl-elimination region along with the global rate constant for the addition−CH_3-elimination process (R1b-2) (obtained by means of eq 7) as a function of temperature are also listed in Table 2.

If we compare the rates constants for the water-elimination and the methyl-elimination processes, it is clear that all the AD

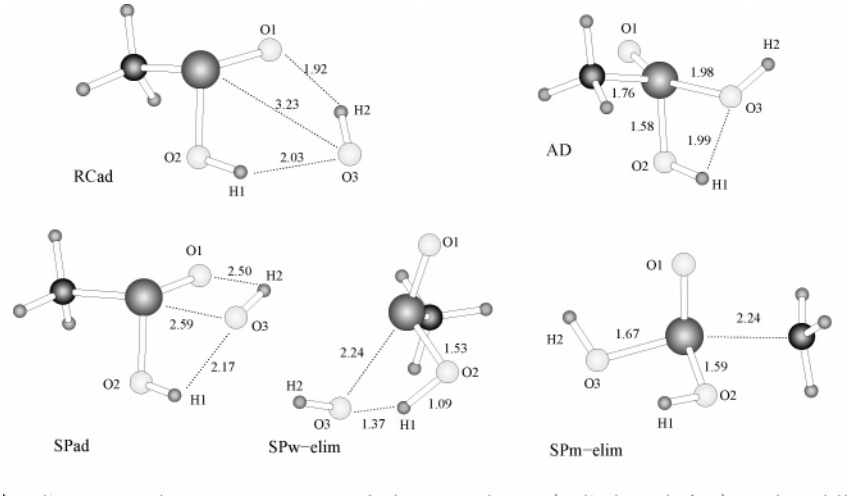

Figure 4. Geometrical representations of the complexes (RCad and AD) and saddle points (SPad, SPw-elim and SPm-elim) along the addition−elimination channel (R1b) for the MSIA + OH reaction. Distances are given in Å and angles in degrees.

TABLE 2: Rate Constants (cm^3 $molecule^{-1}$ s^{-1}) for the Addition−Elimination Channel (R1b) Computed at the CCSD(T)/IB//mPW1K/MG3S Level of Theory[a]

T (K)	$k_{assn-ad}$ (T)	k_{SPad} (T)	k'_{w-elim} (T)	k_{R1b-1} (T)	$k_{SPm-elim}$ (T)	k_{R1b-2} (T)	k_{R1b} (T)
298	1.72 (−09)	3.12 (−10)	1.55 (−09)	1.17 (−14)	3.51 (−05)	2.64 (−10)	2.64 (−10)
325	8.59 (−10)	1.64 (−10)	6.41 (−10)	1.55 (−14)	5.68 (−06)	1.38 (−10)	1.38 (−10)
350	4.99 (−10)	9.95 (−11)	3.20 (−10)	1.97 (−14)	1.35 (−06)	8.29 (−11)	8.30 (−11)
400	2.11 (−10)	4.51 (−11)	1.05 (−10)	2.95 (−14)	1.32 (−07)	3.71 (−11)	3.71 (−11)
450	1.11 (−10)	2.49 (−11)	4.48 (−11)	4.13 (−14)	2.20 (−08)	2.03 (−11)	2.03 (−11)
500	6.77 (−11)	1.58 (−11)	2.30 (−11)	5.48 (−14)	5.34 (−09)	1.27 (−11)	1.28 (−11)
600	3.40 (−11)	8.41 (−12)	8.84 (−12)	8.74 (−14)	6.66 (−10)	6.59 (−12)	6.68 (−12)

[a] Power of ten in parentheses.

TABLE 3: Global Rate Constants (cm^3 $molecule^{-1}$ s^{-1}) Computed at the CCSD(T)/IB//mPW1K/MG3S Level of Theory, and the Contribution of the H-Abstraction Channel to this Rate Constant[a]

T (K)	$k_{MSIA+OH}$ (T)	% H-abs
298	7.67 (−10)	65.6
325	3.94 (−10)	65.0
350	2.34 (−10)	64.5
400	1.02 (−10)	63.6
450	5.47 (−11)	62.9
500	3.37 (−11)	62.1
600	1.70 (−11)	60.8

[a] Power of ten in parentheses.

adduct formed will rapidly decompose into H_2SO_3 and CH_3. This could be expected from the higher barrier found in the water-elimination region (compare the adiabatic potential energies for SPw-elim and SPm-elim). For example, at $T = 298$ K, the water-elimination process is in the range of 10^{-14} cm^3 $molecule^{-1}$ s^{-1}, whereas the methyl elimination is in the range of 10^{-10} cm^3 $molecule^{-1}$ s^{-1}. As a consequence, the rate constant of the addition−elimination channel, $k_{R1b}(T)$, is enterely determined by the methyl-elimination process.

3.3. Global Rate Constant for MSIA + OH. The global rate constant for the reaction between MSIA + OH is obtained by adding the contributions corresponding to the H-abstraction and addition−elimination channels (see eq 2). In Table 3 this rate constant, $k_{MSIA+OH}(T)$, is listed as a function of temperature. Our final value at $T = 298$ K is 7.7×10^{-10} cm^3 $molecule^{-1}$ s^{-1}, somewhat overestimated with respect to the experimental result obtained by Le Bras:[10] $(9 \pm 3) \times 10^{-11}$ cm^3 $molecule^{-1}$ s^{-1}. Nowadays, this is the only experimental value available for the rate constant of the reaction MSIA + OH.

It should be taken into account that this experimental value was obtained by fitting a model involving more than 15 reactions. Some of the rate constants used for those reactions were obtained from literature, others from the same work and others were estimated. Moreover, the model assumed that the only product in reaction R1 was the $CH_3S(O)_2$ radical. However, our rate constant includes the contribution of the addition−elimination channel (R1b), which yields the H_2SO_3 formation. This channel was not taken into account in the experimental model, but its contribution to the global rate constant, at $T = 298$ K, is 34.4%. This high value indicates that it should be included in the models for this reaction.

For that reason, we have also compared the rate constant corresponding just to the $CH_3S(O)_2$ formation (by channel R1a, see Table 1), and neglecting channel R1b-1. Now the value is 5.02×10^{-10} cm^3 $molecule^{-1}$ s^{-1}, still somewhat higher than the experimental value, but noticeably closer.

In Table 3 the contribution of the H-abstraction channel to the global rate constant is listed as a function of temperature. The most relevant result is the important contribution of channel R1b to the global mechanism. As stated before, neither H_2SO_3 nor CH_3 have been detected in the gas phase before as products of the MSIA + OH reaction. For H_2SO_3, this could mean that its decomposition into water and SO_2 is fast enough to contribute to the global production of sulfur dioxide. However, it would be expected that the CH_3 radical is experimentally detected. This could explain the discrepancies between our results and the experimental one,[1] because in their model they were assuming SO_2 as the only product of the reaction, and at $T = 298$ K, 34.4% of the MSIA is reacting with OH via the addition−elimination channel, to form $H_2SO_3 + CH_3$.

As has been previously noted, all the rate constants increase as the temperature decreases. The Arrhenius plot for each individual channel together with the corresponding to the global rate constants are depicted in Figure 5. Although no experi-

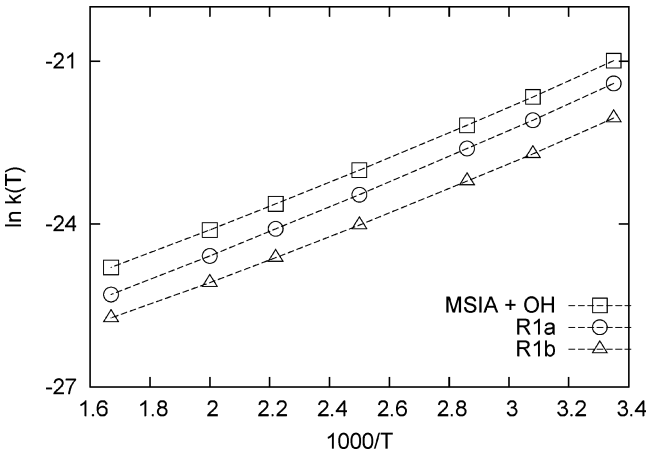

Figure 5. Arrhenius plot for the H-abstraction (R1a) and addition−elimination (R1b) channels, and for the global MSIA + OH reaction. Rate constants in cm^3 $molecule^{-1}$ s^{-1}, and T in K.

mental measurements of the T-dependence for this reaction exist, our results predict a clear negative activation energy. In the range of temperatures studied (298−600 K), the activation energy for the MSIA + OH reaction is −4.49 kcal/mol.

4. Atmospheric Implications

The MSIA oxidation in the atmosphere by reaction with hydroxyl radical seems to be its major degradation pathway. The $CH_3S(O)_2$ radical is the main product formed, with a yield between 65.6% and 60.8% in the range 298−600 K. This means that the other channel, which yields the CH_3 radical, is not negligible.

Ravishankara and co-workers proposed the degradation of the $CH_3S(O)_2$ radical as the key branching point in the cited T-dependence of the SO_4^{2-}/MSA ratio.[18] The authors ruled out the first hypothesis, which proposed that this ratio was controlled by the initial H-abstraction/OH-addition branching in the DMS + OH reaction.[12−14] This hypothesis was based on the fact that MSA was only produced in the OH-initiated addition channel whereas the SO_4^{2-} came from the SO_2 formed in the OH-initiated H-abstraction channel. In this work we have demonstrated that SO_2 is also formed in the addition channel. These theoretical results then help to confirm that the first hypothesis was unfeasible. According then to Ravishankara's new proposal,[18] we have analyzed the competition between unimolecular decomposition of the $CH_3S(O)_2$ radical and its possible bimolecular reactions. Specifically, we have compared the energetic barriers for the S−C bond breaking (to form SO_2) and the OH-addition to form the MSA. Our results support the idea that the reactions of the $CH_3S(O)_2$ radical in the atmosphere could be one key branching point in the T-dependence of the SO_4^{2-}/MSA ratio.

We have built up the different energetic profiles at the CCSD(T)/IB//mPW1K/MG3S (classical and adiabatic potential energy, together with the Gibbs free energy) for the $CH_3S(O)_2 \rightarrow SO_2 + CH_3$ reaction. The adiabatic maximum appears 9.83 kcal/mol above reactants, whereas at $T = 298$ K, the free energy barrier is 8.40 kcal/mol.

Butkovskaya and Setser[51] have recently shown that about the 60% of the reaction exoergicity of the reaction forming $CH_3S(O)_2$ remains in the radical. This percentage is even larger when the $CH_3S(O)_2$ is formed by the indirect mechanism (R1b-1 channel). In these conditions, and with the results obtained, the 60% of 36.82 kcal/mol (which is about 22 kcal/mol) remains in the radical as energy available for dissociation. Taking into account the values previously reported for the energy barriers of the decomposition, the radical would have enough energy to rapidly decompose into CH_3 and SO_2. This would lead to a very low probability of bimolecular reactions of this radical with other species.

However, as the temperature decreases, the energy available for the decomposition decreases, and in consequence increases the number of $CH_3S(O)_2$ radicals stabilized by collisions. Those radicals can react with other species present in the atmosphere: hydroxyl radicals can be added, forming MSA, as proposed by Le Bras and co-workers.[10] We have calculated the classical potential energy profile for this addition process and confirmed that it takes place without a classical potential energy barrier, which means that it will be favored at low temperatures.

In summary, the competition between the unimolecular dissociation of the $CH_3S(O)_2$ radical and the OH-addition would explain the steep temperature-dependent branching ratio between SO_2 and MSA: as the temperature increases the $CH_3S(O)_2$ radical decomposes faster, rapidly decreasing the MSA yield. However, although the $CH_3S(O)_2$ radical influences the SO_4^{2-}/MSA ratio, and when the multiple connections in the DMS + OH degradation scheme are taken into account, we would expect that other species could also influence those field observations.

Acknowledgment. We are grateful for financial support from the Spanish "Ministerio de Educación y Ciencia" and the "Fondo Europeo de Desarrollo Regional" through project No. CTQ2005-07115/BQU, the Generalitat de Catalunya (2005SGR00400) and the use of the computational facilities of the CESCA. N.G.-G. also acknowledges the "Generalitat de Catalunya" for the FI Grant. This paper is dedicated to the memory of Professor Lorenzo Pueyo for his important contributions to Quantum Chemistry.

Supporting Information Available: 1. Energetics for the different regions in the MSIA + OH reaction. 2. High-pressure rate constants. 3. Complete refs 37 and 39 from the main text. This material is available free of charge via the Internet at the http://pubs.acs.org.

References and Notes

(1) Bates, T. S.; Lamb, B. K.; Guenther, A.; Dignon, J.; Stoiber, R. E. *J. Atmos. Chem.* **1992**, *14*, 315.
(2) Shaw, G. E. *Climatic Change* **1983**, *5*, 297.
(3) Charlson, R. J.; Lovelock, J. E.; Andreae, M. O.; Warren, S. G. *Nature* **1987**, *326*, 655.
(4) Barnes, I.; Hjorth, J.; Mihalopoulos, N. *Chem. Rev.* **2006**, *106*, 940.
(5) Yin, F.; Grosjean, D.; Seinfeld, J. H. *J. Atmos. Chem.* **1990**, *11*, 309.
(6) Hertel, O.; Christensen, J.; Hov, Ø. *Atmos. Environ.* **1994**, *15*, 2431.
(7) Sørensen, S.; Falbe-Hansen, H.; Mangoni, M.; Hjorth, J.; Jensen, N. R. *J. Atmos. Chem.* **1996**, *24*, 299.
(8) Arsene, C.; Barnes, I.; Becker, K. H. *Phys. Chem. Chem. Phys.* **1999**, *1*, 5463.
(9) Urbanski, S.; Stickel, R.; Wine, P. *J. Phys. Chem. A* **1998**, *102*, 10522.
(10) Kukui, A.; Borissenko, D.; Laverdet, G.; Le Bras, G. *J. Phys. Chem. A* **2003**, *107*, 5732.
(11) Flyunt, R.; Makogon, O.; Schuchmann, M. N.; Asmus, K.-D.; von Sonntag, C. *J. Chem. Soc., Perkin Trans.* **2001**, *2*, 787.
(12) Berresheim, H. J. *Geophys. Res.* **1987**, *92*, 13.
(13) Legrand, M.; Fenist-Saigne, C.; Saltzman, E. S.; Germain, C.; Barkov, N. I.; Petrov, V. N. *Nature* **1991**, *350*, 144.
(14) Hynes, A. J.; Wine, P. H. In *Biogenic Sulfur in the Environment, edited by Saltzman*, Cooper, W. E., Ed.; American Chemical Society: Washington, DC, 1989.
(15) Hynes, A. J.; Wine, P. H.; Semmes, D. H. *J. Phys. Chem.* **1986**, *90*, 4148.
(16) Barone, S. B.; Turnipseed, A. A.; Ravishankara, A. R. *J. Phys. Chem.* **1996**, *100*, 14694.

(17) Turnipseed, A. A.; Barone, S. B.; Ravishankara, A. R. *J. Phys. Chem*. **1996**, *100*, 14703.
(18) Barone, S. B.; Turnipseed, A. A.; Ravishankara, A. R. *Faraday Discuss.* **1995**, *100*, 39.
(19) González-García, N.; González-Lafont, A.; Lluch, J. M. *J. Comput. Chem*. **2005**, *26*, 569.
(20) González-García, N.; González-Lafont, A.; Lluch, J. M. *ChemPhysChem* **2007**, *8*, 255.
(21) González-García, N.; González-Lafont, A.; Lluch, J. M. *J. Phys. Chem. A* **2006**, *110*, 798.
(22) Hynes, A. J.; Stoker, R. B.; Pounds, A. J.; McKay, T.; Bradshaw, J. D.; Nicovich, J. M.; Wine, P. H. *J. Phys. Chem*. **1995**, *99*, 16967.
(23) Lynch, J.; Fast, P. L.; Harris, M.; Truhlar, D. G. *J. Phys. Chem. A* **2000**, *104*, 4812.
(24) Lynch, B. J.; Zhao, Y.; Truhlar, D. G. *J. Phys. Chem. A* **2003**, *107*, 1384.
(25) Fast, P. L.; Truhlar, D. G. *J. Phys. Chem. A* **2000**, *104*, 6111.
(26) Zhao, Y.; Truhlar, D. G. *J. Chem. Theory Comput.* **2005**, *1*, 415.
(27) Zhao, Y.; González-García, N.; Truhlar, D. G. *J. Phys. Chem. A* **2005**, *109*, 2012.
(28) Zhao, Y.; Truhlar, D. G. *J. Phys. Chem. A* **2005**, *109*, 5656.
(29) Zhao, Y.; Truhlar, D. G. *J. Phys. Chem. A* **2005**, *109*, 4209.
(30) Zhao, Y.; Truhlar, D. G. *Phys. Chem. Chem. Phys*. **2005**, *7*, 2701.
(31) Truhlar, D. G. *Chem. Phys. Lett.* **1998**, *294*, 45.
(32) Fast, P. L.; Sánchez, M. L.; Truhlar, D. G. *J. Chem. Phys*. **1999**, *111*, 2921.
(33) Truhlar, D. G.; Kupperman, A. *J. Am. Chem. Soc*. **1971**, *93*, 1840.
(34) Page, M.; McIver, J. W. *J. Chem. Phys*. **1988**, *88*, 922.
(35) Chuang, Y.-Y.; Corchado, J. C.; Truhlar, D. G. *J. Phys. Chem. A* **1999**, *103*, 1140.
(36) Villá, J.; Truhlar, D. G. *Theor. Chem. Acc*. **1997**, *97*, 317.
(37) Frisch, M. J.; et al. *Gaussian 03*, revision C.02; Gaussian, Inc.: Wallingford, CT, 2004.
(38) Corchado, J. C.; Chuang, Y.-Y.; Coitiño, E. L.; Truhlar, D. G. GaussRate 9.1; University of Minnesota: Minneapolis, MN, 2003; http://comp.chem.umn.edu/gaussrate.
(39) Corchado, J. C.; et al. *PolyRate 9.3*; University of Minnesota: Minneapolis, MN, 2004; http://comp.chem.umn.edu/polyrate.
(40) Garrett, B. C.; Truhlar, D. G. *J. Chem. Phys*. **1979**, *70*, 1593.
(41) Garrett, B. C.; Truhlar, D. G.; Grev, R. S.; Magnuson, A. W. *J. Phys. Chem*. **1980**, *84*, 1730.
(42) Isaacson, A. D.; Truhlar, D. G. *J. Chem. Phys*. **1982**, *76*, 1380.
(43) Truhlar, D. G.; Isaacson, A. D.; Garrett, B. C. *Theory of Chemical Reaction Dynamics*; CRC Press: Boca Raton, FL, 1985; p 65.
(44) Fernández-Ramos, A.; Ellingson, B. A.; Garrett, B. C.; Truhlar, D. G. In *Reviews in Computational Chemistry*; Lipkowitz, K. B., Ed.; Wiley-VCH: Hoboken, NJ, 2006; p 125.
(45) Pechukas, P. *J. Chem. Phys*. **1976**, *64*, 1516.
(46) Garrett, B. C.; Truhlar, D. G. *J. Chem. Phys*. **1982**, *76*, 1853.
(47) Miller, W. H. *J. Chem. Phys*. **1976**, *65*, 2216.
(48) Hirschfelder, J. O.; Wigner, E. *J. Chem. Phys*. **1939**, *7*, 616.
(49) Hu, W.-P.; Truhlar, D. G. *J. Am. Chem. Soc*. **1996**, *118*, 860.
(50) Hu, W.-P.; Truhlar, D. G. *J. Am. Chem. Soc.* **1995**, *117*, 10726.
(51) Butkovskaya, N. I.; Setser, D. W. *Int. Rev. Phys. Chem*. **2003**, *22*, 1.